Microcalorimetry of dust particles in a radio-frequency plasma

Microcalorimetry of dust particles in a radio-frequency plasma

G. H. P. M. Swinkels[a)]
Department of Physics, Eindhoven University of Technology, 5600 MB Eindhoven, The Netherlands

H. Kersten and H. Deutsch
Department of Physics, University of Greifswald, 17487 Greifswald, Germany

G. M. W. Kroesen
Department of Physics, Eindhoven University of Technology, 5600 MB Eindhoven, The Netherlands

(Received 1 November 1999; accepted for publication 13 March 2000)

The internal temperature of rhodamine B-dyed dust particles ($2r_p = 1.2\,\mu$m) immersed in radio-frequency (rf) plasmas has been measured for various plasma conditions. For this purpose, the dye has been excited with an argon-ion laser and the fluorescent emission of the particles has been recorded with an optical multichannel analyzer system. The temperature has been determined after comparison with calibration curves. In argon, the particle temperature increases with rf power and is independent of pressure. In oxygen, an increase with rf power is observed, too. However, the energy flux towards the particles includes also heating by atom recombination (association) and exothermic combustion reactions. These temperature measurements have been compared with calculations based on the thermal balance, where measurements of gas temperature, electron density, and electron temperature have been used. A good agreement between theory and experiment has been found. © *2000 American Institute of Physics.* [S0021-8979(00)03612-4]

I. INTRODUCTION

In the last decade, dusty plasmas attracted a lot of attention. Formation and trapping of dust particles in semiconductor processing plasmas appeared to be a serious source of surface contamination and the main reason for defects in fabricated components resulting in scrapped wafer lots.[1] This lead to an extensive research effort initiated by the semiconductor community to understand particle nucleation, growth, and trapping with the intention to avoid or to reduce particle growth. The increased knowledge and the ability to control the particles in the plasma has recently lead to a line of research—namely, the production of particles with unique and desired qualities. This opens possibilities for, e.g., ceramics and catalysis.[2,3]

In addition to powder formation, also artificially injected powders in plasmas have become an important area of research. In the plasma, the particles acquire a negative charge and the resulting electrostatic particle interactions can result in a spatial arrangement of the particles into regular patterns, which are known as Coulomb crystals.[4,5] A Coulomb crystal can be formed when the ratio of the Coulomb energy to the kinetic energy of the particles exceeds a certain critical value. The formation and structure of the crystal depends on plasma parameters like gas flow rate, radio-frequency (rf) power, gas pressure, and particle parameters like size and size distribution. The Coulomb crystal is an analogy for a solid-state crystal and, therefore, it is used for fundamental studies of, e.g., phase transitions and lattice dynamics. In the last years a number of diagnostics have been applied to dusty plasmas in order to learn more about formation, charging, and other fundamental aspects in the different plasmas.

In addition to the kinetic temperature of a plasma crystal, also an internal temperature of the particles can be distinguished. The behavior of this internal particle temperature T_p is governed by the thermal power balance, which takes into account the several energy fluxes arriving at and leaving from the particle surface, for example, kinetic energy of electrons and ions, ion recombination energy, radical association energy, thermal conduction, radiation, and chemical reaction heat. Measurement of the internal temperature yields valuable information about these different fluxes.

Daugherty has reported one of the few efforts in this direction.[6] He was able to measure the temperature of manganese-activated magnesium fluorogermanate particles in the afterglow of an argon plasma of 300 mTorr and 50 W. To this purpose, the decay time of the phosphorescence of the particles was measured after extinction of the argon plasma. As has been shown by Wickersheim,[7] the decay time is temperature dependent. Daugherty's measurements resulted in a temperature of 410 ± 10 K for the particles.

In other fields, e.g., in fluid mechanics, temperature measurements yield valuable information about combustion processes. Coppeta has shown that dyes like rhodamine B (RhB) can be used to measure temperatures of thermal plumes.[8]

In the present article, we show that the spectral profile of fluorescent emission of melamine–formaldehyde (MF) powders volume dyed with RhB is temperature dependent. We have used these particles to measure real time and *in situ* the internal temperature of these particles while they are suspended in rf plasmas in argon and oxygen, respectively. These two gases are used because they differ in behavior: argon is inert and supplies mainly kinetic energy of charge carriers and their recombination, while oxygen is reactive and supplies, in addition, also other energetic contributions

a)Electronic mail: g.h.p.m.swinkels@phys.tue.nl

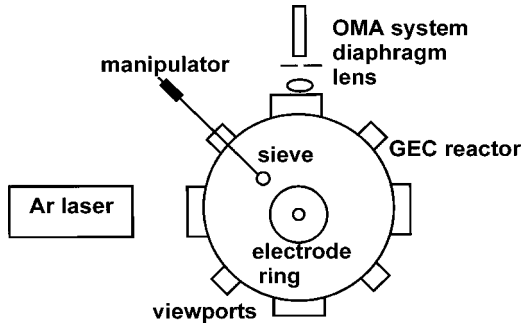

FIG. 1. Experimental setup, schematic.

like chemical reaction energy. Measurements of the internal temperature of the particle combined with data on gas temperature, electron density, and electron temperature will be shown to give good insight into the energy fluxes from plasma to dust particles and, thus, in plasma–particle interactions.

II. EXPERIMENT

A. Equipment

The measurements have been performed in a Gaseous Electronics Conference (GEC) reference cell.[9] Many other researchers, e.g., Olthoff, Hebner, Anderson, Overzet, and McMillin, have used GEC cells to study the behavior of plasmas.[10–14] In our GEC cell we use argon and oxygen as feed gases and we operate between 5 and 60 Pa with a typical flow rate of 1 sccm. The supplied rf power is in the range of 2–45 W. The plasma is created with a frequency generator (Hewlett–Packard 33120A, 13.56 MHz), a wideband rf amplifier (Kalmus 150 C), and a homebuilt T-type matching network. Our GEC cell is equipped with two water-cooled electrodes (one of which is movable), separated by a distance of 6.35 cm. The movable electrode is a showerhead electrode and is used for gas injection. The gas pressure in the cell is maintained by a turbomolecular pump, Edwards EXT250 (He: 250 $\mathrm{l\,s^{-1}}$), and a high vacuum pump, Edwards E2M40 (11.8 $\mathrm{l\,s^{-1}}$). The cell (see Fig. 1 for a schematic picture) has been extended in order to inject dust particles into the plasma. A manipulator arm with a sieve attached allows for the injection of the particles above the center of the powered electrode. An aluminum ring (inner diameter: 20 mm, outer diameter 24 mm, height: 1.5 mm) is used to create a potential trap for the particles just above the powered electrode; the particles are trapped in a fixed and well-known volume.

B. Plasma diagnostics

A commercially available Langmuir probe system (Scientific Systems, SmartProbe) has been used to measure the electron density n_e and the electron temperature kT_e. Furthermore, the system measures the plasma potential V_{pl}, the plasma floating potential V_{fl}, the ion density n_i, the electron energy distribution function (EEDF), and as a result the Debye length λ_D can be calculated. The SmartProbe is an automated Langmuir probe system mounted on an autolinear drive. It consists of a cylindrical conducting tungsten wire that can be inserted into the plasma. The probe is equipped with a high- and a low-frequency plasma potential sensor. The high-frequency sensor compensates for the time-dependent variation of the plasma potential caused by the rf driving voltage. The low-frequency sensor is allowed to float at the plasma floating potential and is used to track and to eliminate any low-frequency dc shifts in the plasma potential. Furthermore, the Langmuir probe system is equipped with a computer program SMARTSOFT that allows for measurement and analysis.

Inserted into the plasma, the wire is dc biased to draw current from the plasma. A current–voltage characteristic is measured and the analysis of the $I-V$ characteristic yields the plasma parameters; typical curves are shown in Fig. 2.

The measured $I-V$ characteristic can be analyzed with a simple probe theory or by the more advanced Laframboise theory that takes the expansion of the sheath around the probe tip into account.[15,16] The electron temperature has been calculated by taking the current measured at the plasma potential and dividing it by the integral of the $I-V$ curve from the floating potential V_f up to the plasma potential V_p:

$$\frac{1}{kT_e}=\frac{I(V_p)}{\int_{V_f}^{V_p} I(V)\,dV}.$$

From the same current also the electron density can be calculated by means of

$$n_e=\frac{I(V_p)}{A_p}\left(\frac{2\pi m_e}{e^2 kT_e}\right)^{1/2}.$$

A diode laser system (Environmental Optical Systems, Inc., LCU-2010-M, ECU-2010-M, with a SN00194 diode) and a BPW 34 photodiode have been used to measure the linewidth of the argon $1s_5$ metastable absorption line (811.5 nm). In our case, the linewidth is determined only by the Doppler width; Stark broadening and Van der Waals broadening are negligible. A measurement of the linewidth, therefore, is directly related to the gas temperature; the density of the $1s_5$ metastables is determined by the surface of the absorption profile. A typical wavelength scan around the 811.5 nm absorption line is shown in Fig. 3; from this scan the absorption profile is calculated. The profile has been fitted with a Gaussian curve. The measurement has been fitted with a Gaussian curve. Absorption profiles have been measured for different pressures and powers, and the related gas temperatures are determined. The results of these measurements are shown in Fig. 4. Furthermore, a height scan has been done: the gas temperature decreases towards the water-cooled electrodes and has a maximum at the sheath-glow boundary, where also the dust particles are confined.

In the case of an oxygen plasma, the radical density n_{O} is important to know in order to estimate the association and reaction of O atoms on the particle surface which may contribute to their thermal balance. Stoffels *et al.*[17] performed calculations on the radical densities in oxygen plasma, which are shown in Fig. 5 for different pressures.

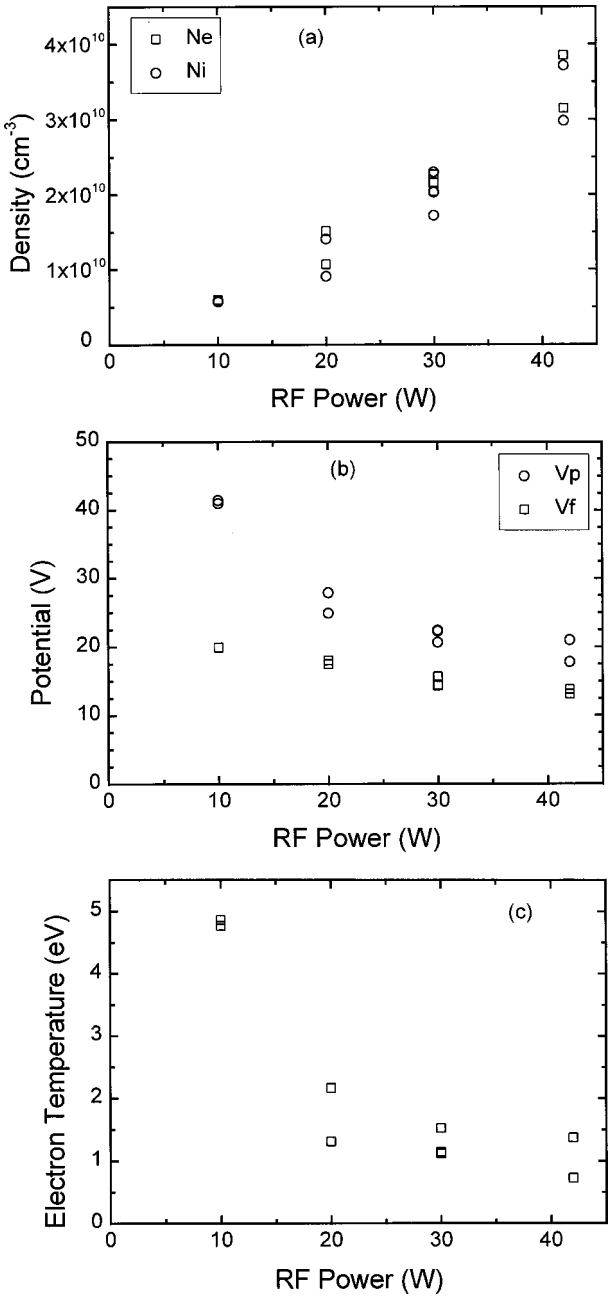

FIG. 2. Electron and ion density (a), plasma and floating potential (b), and electron temperature (c) measured in an argon rf plasma dependent on discharge power. The quantities are measured in the glow for a pressure of $p=20$ Pa.

C. Particle diagnostics

We have used two diagnostics to monitor the particles: fluorescence measurements to determine the particle temperature, and angular-resolved Mie scattering to accurately determine particle size r_p and etch rate $\dot{r}_p$ of the particles.

The particles are injected into the plasma with a manipulator arm (see Fig. 1). The dust is trapped above the powered electrode in an artificial potential trap. The particles are melamine–formaldehyde spheres, which are dyed throughout the volume with rhodamine B (MF/RhB, supplier: Microparticles GmbH, Berlin). The spheres have an original

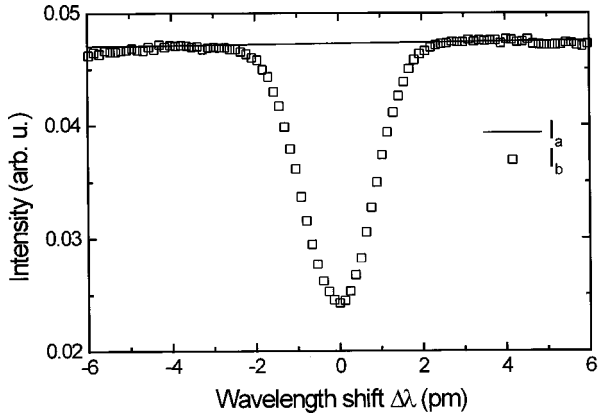

FIG. 3. Typical wavelength scan in an argon plasma ($P=20$ W, $p=20$ Pa, 811.5 nm) used for the determination of the gas temperature. (I_a: intensity assuming no absorption, I_b: measured intensity).

diameter of $2r_p=1.2\,\mu$m, a specific mass density of $\rho=1.51$ g cm^{-3}, and a real refractive index of $n=1.68$; the influence of the RhB on the refractive index is unknown to the authors. The mass fraction m_f of the dye in the spheres is less than 1%. RhB has a boiling point of 210 °C; heating the particles above this temperature leads to a degradation of the dye.

An argon-ion laser (Coherent Innova 70, operated at 514 nm and 28 mW) was used to excite the dyed particles. The resulting fluorescent emission has been recorded using an EG&G optical multichannel analyzer [(OMA) model 1461]. The OMA system has been corrected for the sensitivity of the solid-state detector (EG&G model 1420) using a tungsten ribbon lamp.

For calibration purposes, the spectral behavior of the dyed particles has been recorded as a function of temperature after mixing the particles with oil. The mixture was heated from room temperature to 210 °C. A Fluke 8024A multimeter with thermocouple has been used to monitor the temperature of the mixture. The accuracy of the temperature measurements is 5 °C. As is known from the literature,[18] solvent broadening of the emission curves can occur for dyes. However, in our case the dye is ''solved'' in the particle material and, therefore, the surrounding of the dye is the

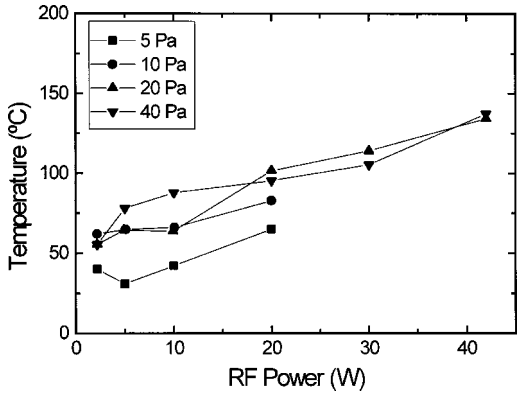

FIG. 4. Argon gas temperature T_g as a function of power for different pressures.

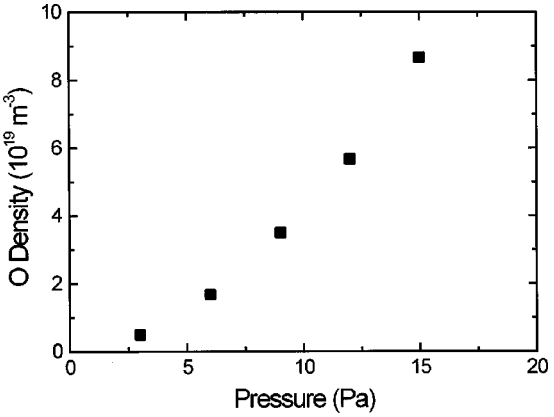

FIG. 5. Oxygen radical density n_O dependent on pressure for experimental conditions as used in the present study (see Ref. 17).

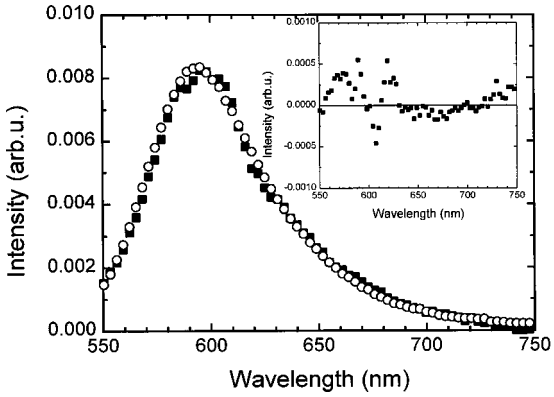

FIG. 7. Fluorescent emission spectra of excited powder particles confined in an argon plasma ($P=42$ W, $p=20$ Pa) in comparison with calibration spectra, and the residue of the curve fit.

same for all cases, whether the particles are suspended in oil or in the plasma.

In Fig. 6 a few calibration curves are shown for the MF/RhB particles we are using. The calibration curves show that the spectral profile of the fluorescent emission depends on the temperature. One can clearly see that as a function of temperature the curve broadens and the intensity decreases. This makes it possible to determine the particle temperature T_p in plasmas without making use of the absolute intensity. This is very convenient: several processes and plasma parameters may hamper reliable measurements of the absolute intensity. The number of trapped particles is not always constant, photobleaching can occur due to laser irradiation, UV lines of the plasma can degrade the dye, and further processes in the plasma, like etching and sputtering, can change the particle and the dye.

Since a laser is used for illumination and excitation of the dust particles in the plasma, the influence of laser heating to the particle has to be estimated. The laser is operated at a power of $P_l=28$ mW and has a beam diameter of $d_l=4$ mm. Only the RhB in the particle will absorb light; the mass fraction of the dye in MF is $m_f=1\%$. The absorption of RhB depends on the excitation wavelength; for 514 nm the absorption relative to the maximum at 550 nm is given by the absorption efficiency $Q_A=0.35$.[8] Also, the quantum yield for fluorescence radiation is important: each photon emitted carries away energy from the particle. In ethanol the quantum yield ϕ, i.e., the ratio of the total energy emitted per quantum of energy absorbed is $\phi=0.69$ according to Guilbault.[18] The laser power, which is absorbed by the MF particle, amounts to $P_l(2r_p/d_l)^2(m_f)^{2/3}Q_A(1-\phi)=51$ pW.

The particles have a mass of $m=8\times10^{-13}$ kg and the specific heat capacity of the MF material is taken to be roughly 10^3 J kg^{-1} K^{-1}. This results in a heat capacity of 0.8 nJ K^{-1} for each particle. The particle temperature T_p will change at a rate of $\partial T_p/\partial t=63$ mK s^{-1}. This ultimately results in an upper limit for the temperature increase of 0.63 K for our measurement time of 10 s. A reduction of quantum yield with temperature, radiation cooling, and Knudsen cooling are not taken into account. Therefore, we estimate the influence of laser heating on the measurements to be negligible.

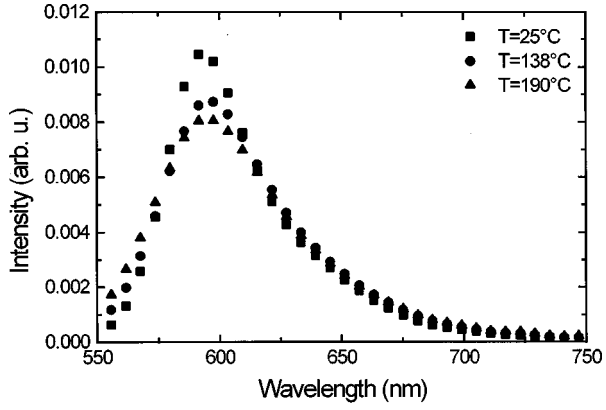

FIG. 6. Spectral profile of MF/RhB fluorescent emission curves for three different temperatures. The dye incorporated into the MF spheres is excited with an argon-ion laser operating at 514 nm and 28 mW.

In the plasma environment, the plasma emission has been recorded before and after exposure of the particles to the laser light and is time averaged to reduce time influences. The averaged emission is then subtracted from the recorded fluorescence spectra during exposure to the laser light. In Fig. 7 an experimental curve is shown and compared to a calibration curve. In the inset of Fig. 7 the residue of the curve fit is plotted. We have chosen for measurements a photon collection time of 10 s in order to enhance the signal-to-noise ratio and to minimize the effect of fluctuations in the plasma emission.

By using the procedure as described above, the particle temperature has been measured in argon and oxygen plasmas. In Figs. 8 and 9 the results for the temperature measurements are shown as a function of rf power. For both gases the particle temperature depends on rf power, but is independent of pressure.

Since the MF particles are being etched in oxygen plasma, angular-resolved Mie scattering has been applied to determine the particle size during the plasma process. This is described in detail elsewhere.[19] The measured scattering spectra are fitted using Mie theory for a single layered homogeneous sphere. In Fig. 10 a typical plot of the particle radius as a function of plasma duration is given. As it can be

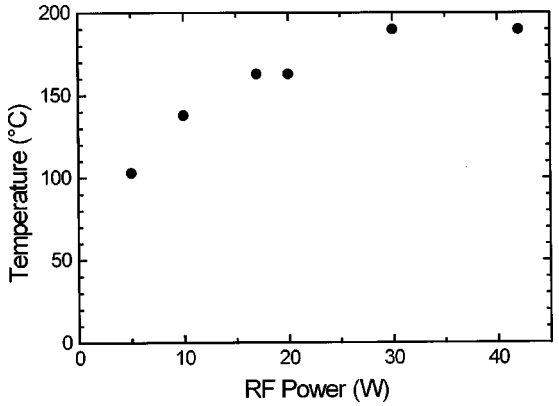

FIG. 8. Measured particle temperature T_p of MF dust confined in a 20 Pa argon rf plasma vs discharge power.

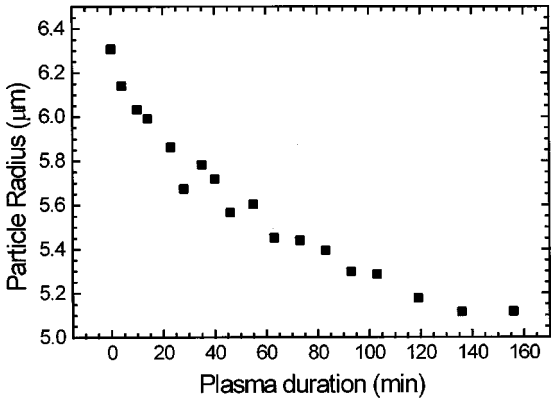

FIG. 10. Example of MF particle etching in oxygen plasma. The etching results in a decrease of the particle radius r_p with increasing process duration ($p=20$ Pa, $P=5$ W).

seen, the particle has been etched in a 20 Pa oxygen plasma operated at 5 W. Simulations indicate that the particle remains spherical for more than 90 min. It is clearly visible that the etch rate decreases with time. In the first 30 s, where also the temperature measurements (T_p) are carried out, the etch rate $\dot{r}_p$ is in the order of 1 nm/s.

III. RESULTS AND DISCUSSION

A. Thermal balance of powder particles confined in a plasma

In practical applications of plasma–particle interactions it is important to know the energy fluxes towards and from particles which result in a certain temperature of the particles. The particle temperature T_p effects elementary processes like adsorption, desorption, and diffusion as well as chemical reactions at the particle surface. For example, the thermal balance of a particle influences its surface properties as stoichiometry, microstructure, etc.[20,21]

The thermal balance of the particles can be written as an equality between the thermal influx Q_{in}, the temporal derivative of the particle enthalpy H_p, and the thermal outflux Q_{out}:

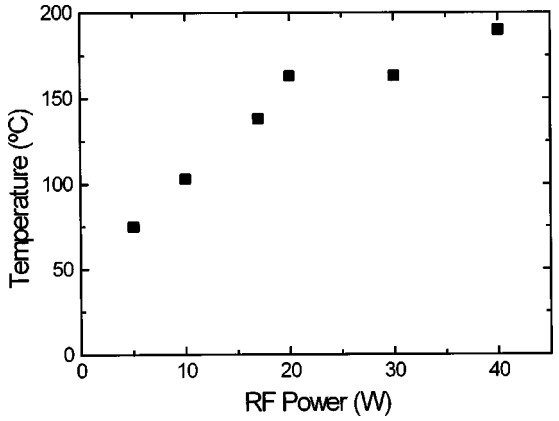

FIG. 9. Measured particle temperature T_p of MF dust confined in a 20 Pa oxygen rf plasma vs discharge power.

$$Q_{\text{in}}=\dot{H}_p+Q_{\text{out}}. \tag{1}$$

In the stationary situation of the particle being suspended in the plasma, $\dot{H}_p=mc(dT_p/dt)=0$. The fluxes Q_{in} and Q_{out} are the surface integrals of the related energy flux densities J_{in} and J_{out}, respectively, over the particles surface A_p: $Q_{\text{in}}=\int_{A_p}J_{\text{in}}dA$ and $Q_{\text{out}}=\int_{A_p}J_{\text{out}}dA$. In the following, the energy flux densities will be discussed in more detail.

In general, the total energy influx J_{in} is the sum of the influxes due to the kinetic energy of electrons (J_e) and ions (J_i), the energy which is released when a positive ion recombines at the surface of the floating particle (J_{rec}), the energy J_{ass}, which is supplied when two gas-phase species (e.g., O atoms) associate into one another gas-phase species at the surface (e.g., O_2 molecule) of the particle, and the energy J_{chem} which is released if a chemical reaction occurs between a gas-phase species and the surface:

$$J_{\text{in}}=J_e+J_{\text{ion}}+J_{\text{rec}}+J_{\text{ass}}+J_{\text{chem}}. \tag{2}$$

Contributions to the energy influx due to laser irradiation and plasma radiation can be neglected in our case as discussed above and because of the relatively low temperature.

The kinetic energetic contributions (J_e,J_i) of the electrons and ions, respectively, are products of the particle fluxes (j_e,j_i) and the mean kinetic energy of the species. Under our experimental conditions, where the diameter $2r_p$ of the particles ($\sim 10^{-6}\,\mu$m) is always small in comparison to the Debye length λ_D ($\sim 10^{-4}\,\mu$m) and the mean-free path λ_{mfp} ($\sim 10^{-2}\,\mu$m), the orbital motion-limited theory for a spherical probe (particle) holds.[16] The electron energy flux density J_e for a Maxwellian electron energy distribution can be calculated by

$$J_e=n_e\sqrt{\frac{k_BT_e}{2\pi m_e}}\exp\left\{\frac{-eV_{\text{bias}}}{k_BT_e}\right\}2kT_e, \tag{3}$$

while the ion energy flux density J_i may be obtained by

$$J_i=n_i\sqrt{\frac{k_BT_i}{2\pi m_i}}\left\{1+\frac{eV_{\text{bias}}}{k_BT_i}\right\}eV_{\text{bias}}. \tag{4}$$

The dust particles rest always at floating potential V_{fl} and it is $V_{\text{bias}}=V_{\text{pl}}-V_{\text{fl}}$. It should be mentioned that the expressions

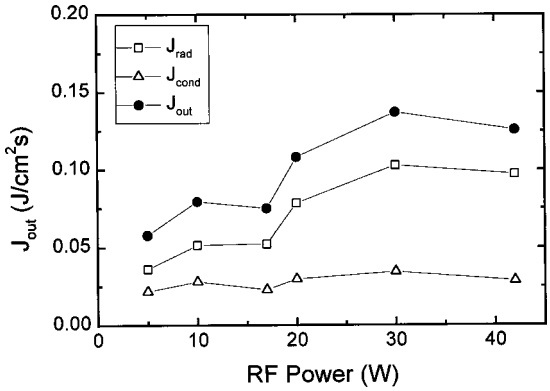

FIG. 11. Energy losses of MF particles in an argon plasma of $p=20$ Pa. The total loss consists of the contribution by radiation and gas convection.

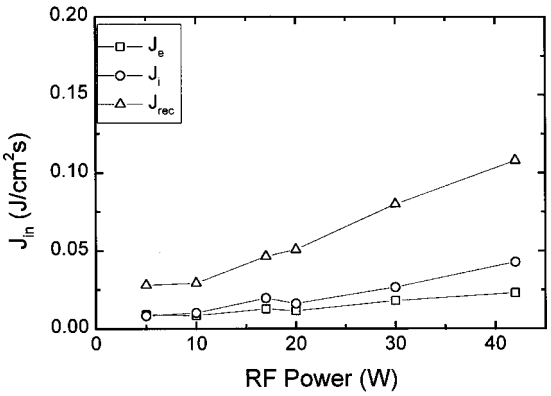

FIG. 12. Different components of the energy influx for an argon plasma consisting of J_e, J_i, and J_{rec}.

for the mean electron energy of $2k_BT_e$ in Eq. (3) are only valid for a Maxwellian electron energy distribution function. If another EEDF holds, one has to modify this contribution. However, in the floating potential V_{fl}, which is the particles potential, the influence of different EEDFs concerning J_e is negligible.[21]

In the case of particles suspended in a plasma, the electron and ion currents towards the particles are equal ($j_e = j_i$) and the released recombination energy flux J_{rec} is

$$J_{\mathrm{rec}} = j_e(E_i - \varphi), \tag{5}$$

where E_i is the ionization energy, which is for argon 15.7 eV. φ is the work function which may be important for metallic particles. In principle, Eq. (5) should be corrected with the difference between the adsorption energy of the ion and the desorption energy of the resulting neutral, but this contribution is rather low.

The energy influx J_{ass} by atom recombination (association) is described by

$$J_{\mathrm{ass}} = \Gamma_{\mathrm{O}} \tfrac{1}{2} n_{\mathrm{O}} \sqrt{\frac{8k_BT_g}{\pi m_{\mathrm{O}}}} E_{\mathrm{diss}}, \tag{6}$$

where Γ_{O} is the association probability of O atoms on the particle surface, T_g is the gas temperature, n_{O} is the density of O atoms, m_{O} is the mass of O atoms, and E_{diss} is the dissociation energy of O_2 molecules. Little is known of the association probability Γ_{O}: it depends on the O-atom surface coverage ratio and the sticking coefficient. A value of 0.05 for Γ_{O} has been estimated for a similar case.[22] For an estimation of the maximum contribution of this effect, we will take $\Gamma_{\mathrm{O}} = 0.1$.

The exothermic chemical reaction (i.e., combustion) energy can be estimated from the etch rate $\dot{r}_p$, the particle material density ρ, and the average specific combustion enthalpy gain h_{comb}:

$$J_{\mathrm{chem}} = \dot{r}\rho h_{\mathrm{comb}}. \tag{7}$$

The outgoing energy flux density J_{out} consists of two contributions: thermal conduction J_{th} by the gas and radiation cooling J_{rad}. In the pressure range considered here, the thermal conduction is governed by the Knudsen theory:[23]

$$J_{\mathrm{th}} = \frac{c_p/c_v + 1}{16(c_p/c_v - 1)} \frac{p}{\sqrt{T_g}} \sqrt{\frac{8k_B}{\pi m}} \alpha(T_p - T_g), \tag{8}$$

where $c_p/c_v = \gamma$ is the heat capacity ratio (adiabatic coefficient), m is the gas molecule mass, p is the gas pressure, k_B is the Boltzmann constant, and α is the accommodation coefficient. The accommodation coefficient accounts for the fact that the desorbing gas atoms or molecules are not necessarily in equilibrium.

The radiation cooling term J_{rad} follows directly from the Stefan–Boltzmann law:

$$J_{\mathrm{rad}} = \epsilon\sigma(T_p^4 - T_g^4), \tag{9}$$

where ϵ denotes the emissivity, and σ is the Stefan–Boltzmann constant ($\sigma = 5.67 \times 10^{-8}\ \mathrm{W\,m^{-2}\,K^{-4}}$).

B. Argon plasma

In the stationary case where the particles are heated to their equilibrium temperature T_p, the energy fluxes are equal: $J_{\mathrm{in}} = J_{\mathrm{out}}$. Hence, by knowledge of the outgoing flux J_{out}, which consists of the thermal conduction J_{th} and the radiation J_{rad}, the total energy flux towards a powder particle can be obtained and compared with model calculations.

In accordance with Eqs. (8) and (9) the loss terms are essentially determined by the particle temperature T_p and the gas temperature T_g which have been measured, see Figs. 4, 8, and 9. For argon the adiabatic coefficient is $\gamma = 5/3$ and the accomodation coefficient $\alpha = 0.86$ has been suggested in the literature.[20] The emissivity of the polymer-like MF particles is supposed to be 0.9.[24] By using these values the energy losses by gas cooling and heat radiation of a particle suspended in an argon rf plasma are calculated. The results are shown in Fig. 11. For the used pressure of 20 Pa the cooling by radiation is stronger than the cooling by the gas convection. This observation is in agreement with other authors.[25]

In Fig. 12 the calculated components Eq. (2) for the energy influx J_{in} are depicted: the energy influx consists of J_e, J_i, and J_{rec}. In the case of an argon plasma only the energetic contributions due to kinetic energy of the charge carriers [Eqs. (3) and (4)] and their recombination [Eq. (5)] have to be considered; the recombination clearly dominates

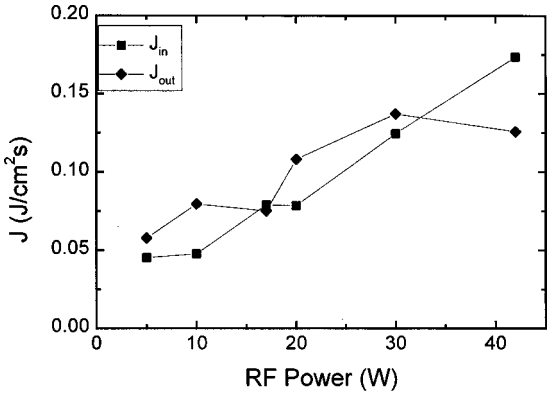

FIG. 13. Comparison of the calculated energy influx J_{in} with the measured energy loss J_{out} for an argon plasma of 20 Pa.

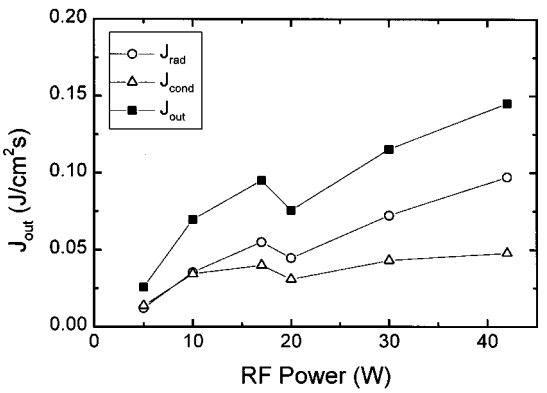

FIG. 14. Energy losses of MF particles in an oxygen plasma of $p=20$ Pa. The total loss consists of the contribution by radiation and gas convection.

the energy influx. Because of the inert gas behavior the contributions due to molecule association and chemical reactions with the particle surface can be neglected. In order to calculate J_e, J_i, and J_{rec} the internal plasma parameters obtained by Langmuir probe measurements (see Fig. 2) and/or typical literature values for a GEC cell under comparable experimental conditions,[13,26,27] respectively, have been taken.

In Fig. 13 the energy influx has been compared with the determined outflux J_{out} based on the temperature measurements. As can be seen in Fig. 13, the calculated energy influx is in quite good agreement with the measured values of J_{out}. Since the MF particles are at floating potential, the heating by kinetic energy of the Ar^+ ions and electrons is small due to the rather small potential drop between the plasma and floating potential. The dominant contribution is the recombination of the charge carriers.

Because the material constants as the accomodation coefficient α and the thermal emissivity ϵ of the particles linearly go down in the determination of the outgoing energy flux, the accuracy of J_{out} depends on the knowledge of those coefficients which have been taken from the literature.[20,24] However, the coefficients do not exhibit a strong variation if one looks to slightly changed experimental conditions. Therefore, the taken values seem to be reliable. The results indicate that a description of the energy influx by charge carriers, which are characterized by plasma diagnostics, is an appropriate tool for the treatment of plasma–particle interaction. On the other hand, the use of microparticles as thermal probes in an argon plasma has been successfully demonstrated.

C. Oxygen plasma

During oxygen plasma treatment of the hydrocarbon/nitrogen-containing MF particles ($C_3H_6N_6$ and CH_3O highly cross-linked molecule), the energy fluxes towards the substrates have been determined by measurements of T_p in the same way as for argon. However, now the contributions to the total energy influx in addition to the kinetic ion energy transfer are also due to recombination of atomic species (association) and exothermic combustion reactions of the plastic-like particles by the plasma-generated oxygen radicals.[28] Etching of the particles confirms the chemical reaction process that may be attributed to the following mechanisms:

(i) Chemical surface film reactions of the particle surface layers with oxygen atoms which are produced in the collision-dominated sheath region and in the negative glow by dissociation of O_2 molecules, and
(ii) chemical sputtering by high energetic O_2^+ and O^+ species colliding with the particles.

However, the latter as well as physical sputtering of the particle surface are less important. Since the particles are at floating potential, the energy for efficient sputtering is too low. Otherwise, also in the inert argon plasma, particle etching would be observed. But even for very long process times ($t>30$ min), in this case the particle size was constant as measured by Mie scattering ellipsometry and angular-resolved forward scattering. Hence, plasma etching of confined MF particles will proceed only by the chemically reactive oxygen radicals and ions.

By using the measured particle temperature T_p (see Fig. 9) the energy loss has been estimated again according to Eqs. (8) and (9). For oxygen in Eq. (8) the adiabatic coefficient is $c_p/c_V=7/5$ and the accommodation coefficient has been taken in accordance with Ref. 29 as $\alpha=0.9$. During etching the emissivity of the particle does not change, therefore, it remains $\epsilon=0.9$ in Eq. (9). The results for the particles energy loss J_{out} in an oxygen plasma as a function of power are shown in Fig. 14. Similarly to the argon plasma, for low pressures ($p=20$ Pa) the cooling by radiation is dominant, too.

As described above, the loss has to be balanced by the incoming contributions with regard to particle heating due to charge carriers and radical association and chemical reaction. The particle density r_O of the oxygen atoms is mainly determined by electron-impact processes taking place in the glow region:

$$O_2+e_f\rightarrow O_2^+ +2e,$$

$$O_2+e_f\rightarrow O^+ +O+2e,$$

$$O_2+e_f\rightarrow O+O+e.$$

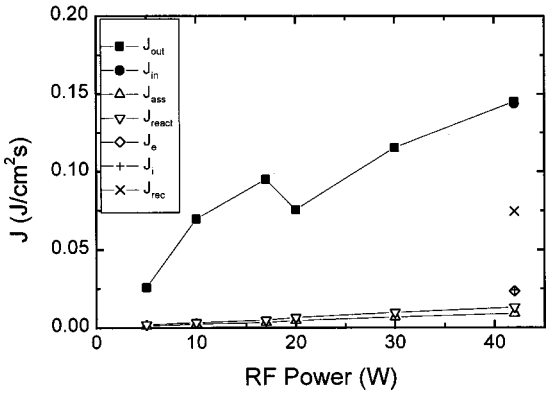

FIG. 15. Comparison of the calculated energy influx for an oxygen plasma J_{in} consisting of J_e, J_i, J_{rec}, J_{ass}, and J_{chem} with the measured energy loss J_{out} as determined in Fig. 14.

The abbrevation e_f stands for fast beam electrons released by secondary electron emission at the cathode (γ process).[30] The low-energy plasma electrons (e_l), which exist in the glow in a rather high density, generate preferably negative molecule ions by electron attachment. However, they decay into more stable negative atom ions and oxygen atoms, respectively,

$$O_2 + e_l \rightarrow O_2^-,$$

$$O_2^- \rightarrow O^- + O,$$

$$O_2^- \rightarrow O + O + e.$$

The preferred generation of negative ions also contributes to the formation of oxygen atoms by charge exchange:

$$O^- + O_2 \rightarrow O + O_2^-,$$

$$O^- + O_2 \rightarrow O^+ + O_2 + 2e.$$

The efficiency of oxygen ionization and dissociation depends on the electron energy distribution function and the electron density. Both are strongly influenced by the power and gas pressure in the discharge. Unfortunately, there are only complete data sets of the plasma parameters available for high power. The dissociation degree, which is in the order of 0.01–0.05 under our experimental conditions, results in values for n_{O} of about $2\times10^{20}\,\text{cm}^{-3}$ (Fig. 5). The other quantities which are necessary to calculate the contribution J_{ass} in Eq. (6) are: $E_{\text{diss}}=5\,\text{eV}$ and $\Gamma_{\text{O}}=0.12$. Under these assumptions, the contribution of oxygen radical association to the total heat flux is in the order of 5%, as indicated in Fig. 15.

The rather high inflow of oxygen atoms towards the substrate leads also to reactions with the MF particles surface. The surface density of atoms of the MF particles is in the order of 10^{14}–$10^{15}\,\text{cm}^{-2}$. Thus, the relatively high particle influx results in surface reactions with oxygen even if the sticking probability of the reactive atoms at the MF surface should be small. The removal (etching) of the products is influenced by the thermal conditions at the surface.

The MF particles are polymerized $C_3H_6N_6$ molecules. The combustion heat of this material is 2.16×10^4 kJ/kg (Ref. 31) and the heat released by combustion has been determined according to Eq. (7) to be in the order of 5%, which is comparable to the contribution by association, see Fig. 15. However, as in the case of an argon plasma, the recombination of positive ions and electrons is again the dominating part in the energy balance of a particle confined in an oxygen plasma.

IV. CONCLUSIONS

We have demonstrated that *in situ* laser-induced fluorescence of dyed dust particles allows for a determination of the internal particle temperature. If these measurements are combined with measurements of the electron density, electron temperature, gas temperature, and particle etch rate, all input parameters of the thermal balance of the particles are known. The dominant heating mechanisms for argon plasmas are particle heating due to charge-carrier recombination. For oxygen plasmas, also a small contribution due to radical recombination of oxygen atoms to molecules is important. Both loss mechanisms, heat conduction and radiation cooling, are of equal importance. The calculated influx and outflux agree quite well.

In short, the *in situ* thermometry method in this article actually turns the suspended particles into microprobes for the particle energy balance, and indirectly also to microprobes for the balance between the several plasma–surface interaction mechanisms.

ACKNOWLEDGMENTS

This work is part of the research program of the ''Stichting voor Fundamenteel Onderzoek der Materie (FOM),'' which is financially supported by the ''Nederlandse Organisatie voor Wetenschappelijk Onderzoek (NWO).'' Part of the work has been supported by the Netherlands Technology Foundation (STW) and the Deutsche Forschungsgemeinschaft (DFG) under SFB198/A14. One of the authors (H.D.) is indebted to NWO and the Alexander von Humboldt Stiftung for their joint support. The authors wish to express their thanks to Loek Baede.

[1] G. M. W. Kroesen, Phys. World **9**, 25 (1996).
[2] H. Hofmeister, J. Duta, and H. Hofmann, Phys. Rev. B **54**, 2856 (1996).
[3] H. Kersten, P. Schmetz, and G. M. W. Kroesen, Surf. Coat. Technol. **108-109**, 507 (1998).
[4] A. Melzer, A. Homann, and A. Piel, Phys. Rev. E **53**, 2757 (1996).
[5] H. Thomas, G. E. Morfill, V. Demmel, J. Goree, B. Feuerbacher, and D. Möhlmann, Phys. Rev. Lett. **73**, 652 (1994).
[6] J. E. Daugherty and D. B. Graves, J. Vac. Sci. Technol. A **11**, 1126 (1993).
[7] K. A. Wickersheim and M. H. Sun, J. Microwave Power **22**, 85 (1987).
[8] J. Coppeta and C. Rogers, Exp. Fluids **25**, 1 (1998).
[9] P. J. Hargis, Jr., K. E. Greenberg, P. A. Miller, J. B. Gerardo, J. R. Torczynski, M. E. Riley, G. A. Hebner, J. R. Roberts, J. K. Olthoff, J. R. Whetstone, R. J. Van Brunt, M. A. Sobolewski, M. Anderson, M. P. Splichal, J. L. Mock, P. Bletzinger, A. Garscadden, R. A. Gottscho, G. Selwyn, M. Dalvie, J. E. Heidenreich, J. W. Butterbaugh, M. L. Brake, M. L. Passow, J. J. Pender, A. Lujan, M. E. Elta, D. B. Graves, H. H. Sawin, M. J. Kushner, J. T. Verdeyen, R. Horwath, and T. R. Turner, Rev. Sci. Instrum. **65**, 140 (1994).
[10] J. K. Olthoff and K. E. Greenberg, J. Res. Natl. Inst. Stand. Technol. **100**, 327 (1995).
[11] G. A. Hebner, J. Appl. Phys. **80**, 2624 (1996).
[12] H. M. Anderson and S. B. Radovanov, J. Res. Natl. Inst. Stand. Technol. **100**, 449 (1995).
[13] L. J. Overzet and M. B. Hopkins, J. Appl. Phys. **74**, 4323 (1993).
[14] B. K. McMillin and M. R. Zachariah, J. Appl. Phys. **77**, 5538 (1995).

[15] Scientific Systems, SmartProbe technical notes.
[16] J. E. Allen, Phys. Scr. **45**, 497 (1992).
[17] E. Stoffels, W. W. Stoffels, D. Vender, M. Kando, G. M. W. Kroesen, and F. J. de Hoog, Phys. Rev. E **51**, 2425 (1995).
[18] G. Guilbault, *Practical Fluorescence: Theory Methods and Techniques* (Marcel Dekker, New York, 1973).
[19] W. W. Stoffels, E. Stoffels, G. H. P. M. Swinkels, M. Boufnichel, and G. M. W. Kroesen, Phys. Rev. E **59**, 2302 (1999).
[20] R. Piejak, V. Godyak, B. Alexandrovich, and N. Tishchenko, Plasma Sources Sci. Technol. **7**, 590 (1998).
[21] H. Kersten, G. M. W. Kroesen, and R. Hippler, Thin Solid Films **332**, 282 (1998).
[22] E. Meeks, P. Ho, A. Ting, and R. J. Buss, J. Vac. Sci. Technol. A **16**, 2227 (1998).
[23] M. Knudsen, Ann. Phys. (Leipzig) **34**, 593 (1911).
[24] *CRC Handbook of Chemistry and Physics*, 75th ed., edited by P. R. Lide and H. P. R. Frederikse (CRC, Boca Raton, FL, 1994).
[25] R. J. Visser, J. Vac. Sci. Technol. A **7**, 189 (1989).
[26] K. E. Greenberg and G. A. Hebner, J. Appl. Phys. **73**, 8126 (1993).
[27] J. K. Olthoff, R. J. Van Brunt, S. B. Radovanov, J. A. Rees, and R. Surowiec, J. Appl. Phys. **75**, 115 (1994).
[28] H. Kersten, H. Deutsch, and J. F. Behnke, Vacuum **48**, 123 (1997).
[29] G. R. Somorjai, *Introduction to Surface Chemistry and Catalysis* (Wiley, New York, 1994).
[30] Ph. Belenguer and J. P. Boeuf, Phys. Rev. A **41**, 4447 (1990).
[31] The combustion heat of MF has been calculated on the basis of a code. Thanks are due to H. Wulff, Department of Chemistry, University of Greifswald.